Supporting Information

Bröcker et al. 10.1073/pnas.1117797109

SI Experimental Procedures

Yeast Strains. All yeast strains are listed in Table S2.

Yeast Cell Culture. Two liters of YP medium were supplemented with 2% (vol/vol) D-galactose and 8 mL of a preculture grown overnight in YPG. Cells were harvested after 48 h of growth and addition of 1% (vol/vol) D-galactose after 24 h. After washing in H_2O and buffer [300 mM NaCl, 50 mM Hepes/NaOH (pH 7.5) with protease inhibitors (1xFY; Serva) and 1 mM PMSF], cells were frozen in liquid nitrogen and stored at −80 °C.

Tandem Affinity Purification and Pull-Down Assays. Purification of homotypic fusion and vacuole protein sorting (HOPS) complex and HOPS subcomplexes was done via the tandem affinity purification (TAP) protocol as previously described (1). For preparation of HOPS for EM analyses, the buffer was as follows: 1 M NaCl, 50 mM Hepes/NaOH (pH 7.5), and 10% (vol/vol) glycerol. HOPS subcomplexes were purified in 300 mM NaCl. Tobacco etch virus (TEV)-eluted complexes were resolved on 10–30% glycerol gradients that were centrifuged for 18 h at 4 °C in a SW40 rotor at 283,000 × *g*. Fractions of 340 μL were collected from the top of the gradient and further analyzed for fusion or EM. Where indicated, glutardialdehyde was added to the gradient to stabilize the HOPS complex (2). GST pull-downs were performed as previously described (1), except that buffers were supplemented with 150 mM NaCl and 7 mg/mL fatty acid-free BSA in the loading and washing buffer.

Fluorescence Microscopy. For GFP/FM4-64 microscopy, yeast cells were grown overnight in YPG or YPD, diluted, and grown to log-phase in YPG or YPD. Staining of the cells with FM4-64 was performed as previously (1). Afterward, cells were resuspended in selective complete medium with D-glucose or D-galactose, respectively, and analyzed with a Leica DM5500B microscope equipped with a SPOT Pursuit camera using GFP, FM4-64, and differential interference contrast (DIC) filters. Exposure times for GFP and FM4-64 were 150 ms and 100 ms, respectively. Pictures were processed by using Adobe Photoshop CS3 and deconvoluted with Autoquant.

Vacuole Fusion Assay. Vacuole fusion was performed with vacuoles from two tester strains, in which the endogenous *VPS11* gene was replaced by a temperature-sensitive *vps11-1* allele (3). Fusion was measured by a complementation assay. One tester vacuole contains alkaline phosphatase (Pho8) but lacks its processing peptidase Pep4. The other contains Pep4 but lacks Pho8. Upon fusion, Pep4 processes Pho8 to the active enzyme. Fusion activity is determined by measuring the dephosphorylation of p-nitrophenol–phosphate. Because of the *vps11-1* allele on both vacuole types, fusion only occurs after the addition of purified HOPS (3).

Glycerol Gradient Centrifugation—GraFix. Glycerol gradient centrifugation with simultaneous cross-linking with glutardialdehyde was performed according to Kastner et al. (2). Glycerol gradients [10–30% (vol/vol) glycerol] in 11 × 60-mm tubes (Beckman Instruments) with or without a glutardialdehyde gradient from 0 to 0.25% were centrifuged for 18 h at 283,000 × *g* using a SW40 rotor (Beckman Instruments). Fractions were harvested and analyzed by EM or added to the vacuole fusion assay.

EM and Image Processing. ***Sample preparation and image recording.*** Samples were either directly prepared for EM as previously described (4) or first cross-linked on a glycerol gradient as described above. In brief, 6 μL of the cross-linked samples were absorbed for 1–3 h at 4 °C and 100% humidity to a freshly glow-discharged copper grid (Agar Scientific; G2400C) covered by a thin, continuous carbon film. Excess sample was blotted using filter paper (Whatman no. 4). After washing twice with ddH_2O and staining with 0.07% uranyl formate (SPI Supplies/Structure Probe) for 1 min, the grid was air-dried and ready to use.

All images were taken with a JEOL JEM-1400 electron microscope equipped with an LaB_6 filament at an operation voltage of 120 kV. Images of wild-type HOPS, HOPS (VPS39-GFP), HOPS (VPS33-GFP), and the respective subcomplexes were either collected on Kodak S0-163 film or were recorded with a 4k × 4k CCD camera F416 (TVIPS) using low-dose conditions. Micrographs were digitized by using a Heidelberg Tango drum scanner with a 10.5-μm step size, yielding a pixel size of 2.1 Å on the specimen level. Digital micrographs were recorded at calibrated magnifications of 53,800× and 67,200×, resulting in a pixel size of 2.9 Å and 2.3 Å, respectively.

2D alignment. Approximately 24,900 HOPS (Vps39-GFP) particles were collected from 920 electron micrographs using boxer (5). Only particles that clearly represented full-length complexes were selected. For the subcomplexes Vps16-Vps33 we analyzed 28,000 particles from 300 images, for Vps39-Vps11-Vps18 9,000 particles from 400 images, and for Vps39-Vps11 3,200 particles from 65 images. For wild-type HOPS with and without cross-linking we analyzed 9,500 and 14,300 particles from 135 and 202 images, respectively. For HOPS (Vps33-GFP) 6,500 particles were selected from 405 images. The images were aligned and classified using reference-free alignment and *k*-means classification procedures implemented in SPARX and EMAN2 (6).

To properly align the full HOPS complex, images were first centered at the head region, using a circular model image with the proper radius as reference and then rotationally aligned, excluding the stem and tail domains. This strategy produced a global average in which only the head and the upper part of the stem was visible. Subsequent *k*-means classification was performed within a mask encompassing the head only. The obtained class averages showed a high amount of details in the head region, whereas the stem and tail appeared blurred. A second round of classification was then performed within each subset, using a mask excluding the head but including all positions of the stem and tail. This approach produced classes with clearly defined structures of head, stem, and tail. Selected class averages were then sorted manually into a sequence suitable for a movie.

3D reconstructions. For the 3D reconstruction of HOPS (Vps39-GFP), image pairs were collected at tilt angles of 50° and 0°, and 4,800 particle pairs were selected from 200 image pairs using WEB, the display program associated with the SPIDER software package (7), which was used for further image-processing steps. The 4,800 untilted particles were then submitted to several rounds of multireference alignment. Thirty selected class averages obtained in the previous step were used as starting references. Random conical tilt reconstructions of the tilted particles were calculated from the seven best class averages by back-projection, followed by back-projection refinement. The resulting reconstructions were then submitted to several rounds of 3D multireference projection matching against the dataset of 24,900 single particles using SPARX. The initial angular increment was 15°, and subsequent refinement rounds were performed with decreasing angular steps. Four reconstructions remained stable during the refinement process with a resolution of ≈29 Å ac-

cording to the 0.5 criterion (Fig. S6). The respective classes contained between ≈3,000 and ≈7,000 particles.

For the 3D reconstruction of Vps16-Vps33, we collected 88 image pairs, from which 4,260 particle pairs were selected. For the subcomplexes Vps39-Vps11-Vps18 and Vps39-Vps11, we selected 3,250 and 4,260 particle pairs from 102 and 88 image pairs, respectively. Particle images were aligned, and 3D reconstructions were calculated from representative class averages using the same approach as described for the full HOPS complex. The final reconstructions contained ≈600 (Vps16-Vps33), ≈200 (Vps39-Vps11-Vps18), and ≈360 (Vps39-Vps11) particles and had resolutions between 20 and 40 Å (Fig. S6).

For visualization, analysis, and preparation of the figures, we used Chimera (8). Initial segmentation of the HOPS complex was performed automatically using the module Segment Map of the Chimera software package (9). The segmentation results were then manually optimized, taking the fitting of the subcomplexes into account. Morphing between the four different density maps was computed with the Morph Map module of the Chimera software and recorded as a movie.

Antibody labeling. To locate subunits in the HOPS complex, we labeled HOPS (Vps33-GFP), HOPS (Vps39-GFP), HOPS (Vps39-CbP) (wild type), and HOPS subcomplex Vps39-CbP-Vps11-Vps18 with anti-GFP and anti-CbP antibodies, respectively (CbP = Calmodulin-binding peptide). After incubation at a ratio of 1:50 for 1 h at 4 °C, labeled complexes were cross-linked and separated using a glycerol gradient. Single-particle datasets were obtained as described above, and approximately 100 particles showing a clear additional density were manually selected for each data set. The data sets were submitted to reference-free alignment and *k*-means classification (40–50 particles per class) using SPARX. The best class averages were selected (each containing ≈10 particles) and illustrated at higher threshold, to demonstrate that the antibody densities are well defined against the background.

Gold labeling. To determine the position of HOPS Ypt7 binding, TAP-purified HOPS complexes and 150 μg purified His_6-tagged Ypt7, preloaded with GTPγS according to Ostrowicz et al. (1), was incubated at 1:1 ratio for 1 h at 4 °C. After subsequent cross-linking by glutardialdehyde and separation on a glycerol gradient, the sample was applied to a normal carbon-coated copper grid. After 1 h of incubation the grid was washed with water and placed on a droplet of 5 nm Ni-NTA-nano-gold (Nanoprobes) for 1 min. The grid was then incubated for 1 min in buffer containing 60 mM Hepes (pH 7.4), 300 mM NaCl, and 10 mM imidazole, washed twice with water, and then stained with uranyl formate as described above.

Tomography. To verify that HOPS complexes were not flattened using negative stain, we also collected several tomograms of negatively and cryo-negatively stained complexes according to the described protocol (4). Images were taken with the JEOL JEM-3200FSC electron microscope equipped with a field-emission gun at an operation voltage of 200 kV. An energy filter was used with a slit width of 12 eV. The tomograms were recorded with an 8k × 8k CMOS-camera F816 (TVIPS), with binning the pictures twice. The grid was tilted from −52° to 52° incrementing in 2° steps, and an electron dose of 1 $e^-/Å^2$ per picture was applied. Tilt series images were aligned and reconstructed using the weighted back-projection method as implemented in the IMOD software package (10). Volumes of the HOPS complex were extracted in Chimera (8) and filtered at 35 Å using a Gaussian low-pass filter.

1. Ostrowicz CW, et al. (2010) Defined subunit arrangement and rab interactions are required for functionality of the HOPS tethering complex. *Traffic* 11:1334–1346.
2. Kastner B, et al. (2008) GraFix: Sample preparation for single-particle electron cryomicroscopy. *Nat Methods* 5:53–55.
3. Stroupe C, Collins KM, Fratti RA, Wickner W (2006) Purification of active HOPS complex reveals its affinities for phosphoinositides and the SNARE Vam7p. *EMBO J* 25: 1579–1589.
4. Ohi M, Li Y, Cheng Y, Walz T (2004) Negative staining and image classification—powerful tools in modern electron microscopy. *Biol Proced Online* 6:23–34.
5. Ludtke SJ, Baldwin PR, Chiu W (1999) EMAN: Semiautomated software for high-resolution single-particle reconstructions. *J Struct Biol* 128:82–97.
6. Hohn M, et al. (2007) SPARX, a new environment for Cryo-EM image processing. *J Struct Biol* 157:47–55.
7. Frank J, et al. (1996) SPIDER and WEB: Processing and visualization of images in 3D electron microscopy and related fields. *J Struct Biol* 116:190–199.
8. Pettersen EF, et al. (2004) UCSF Chimera—a visualization system for exploratory research and analysis. *J Comput Chem* 25:1605–1612.
9. Pintilie GD, Zhang J, Goddard TD, Chiu W, Gossard DC (2010) Quantitative analysis of cryo-EM density map segmentation by watershed and scale-space filtering, and fitting of structures by alignment to regions. *J Struct Biol* 170:427–438.
10. Kremer JR, Mastronarde DN, McIntosh JR (1996) Computer visualization of three-dimensional image data using IMOD. *J Struct Biol* 116:71–76.

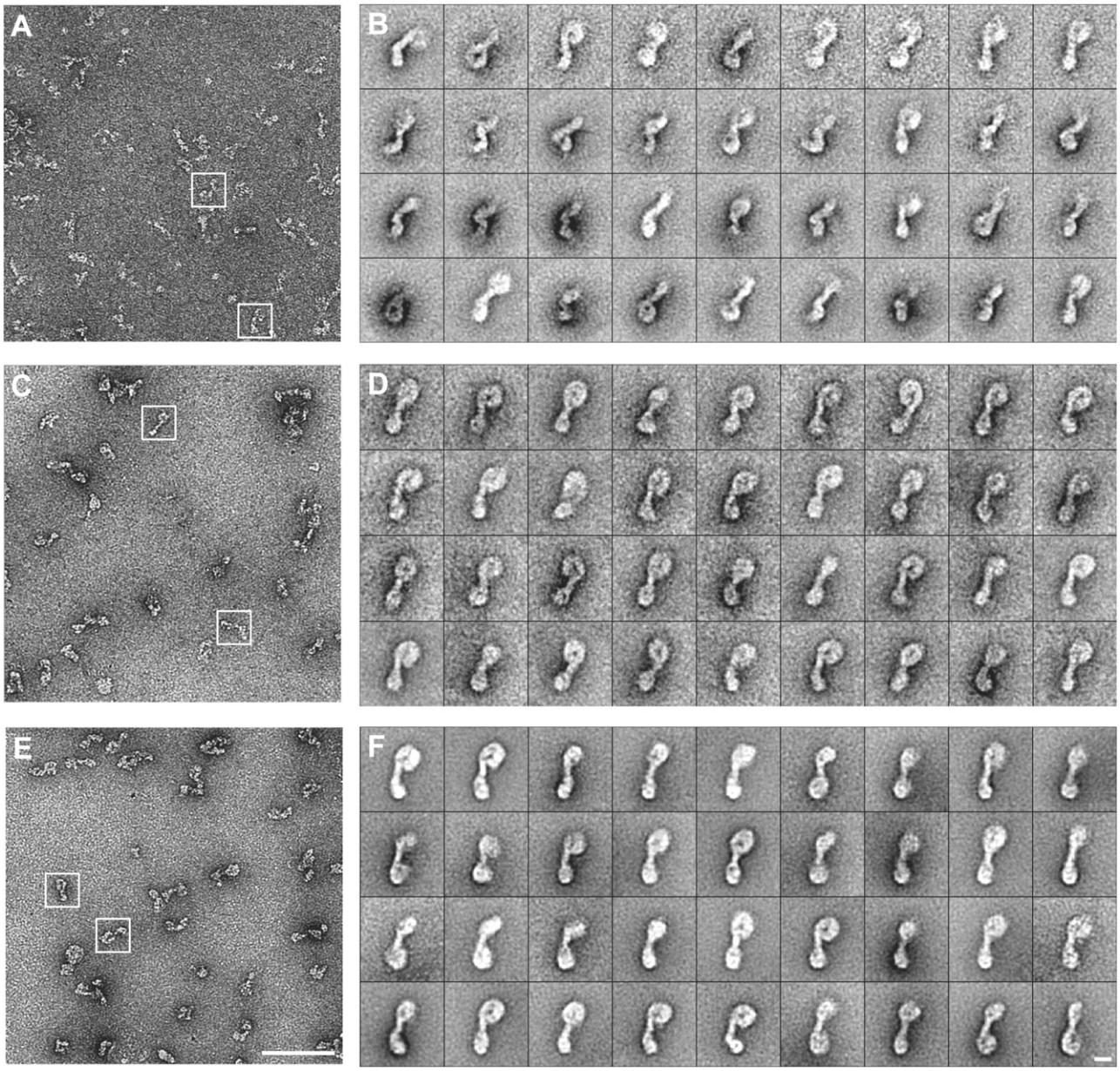

Fig. S1. Comparison of differently labeled and prepared HOPS complexes. (*A* and *B*) Wild-type HOPS, (*C* and *D*) cross-linked wild-type HOPS, and (*E* and *F*) cross-linked HOPS (Vps33-GFP) were negatively stained, imaged, and processed as described in *SI Experimental Procedures*. (*A*, *C*, and *E*) Typical micrograph areas of the negatively stained HOPS complexes. Representative particles are boxed in white. (Scale bar, 100 nm.) (*B*, *D*, and *F*) Representative class averages, containing 13–82, 11–30, and 15–107 particles, respectively. (Scale bar, 10 nm.)

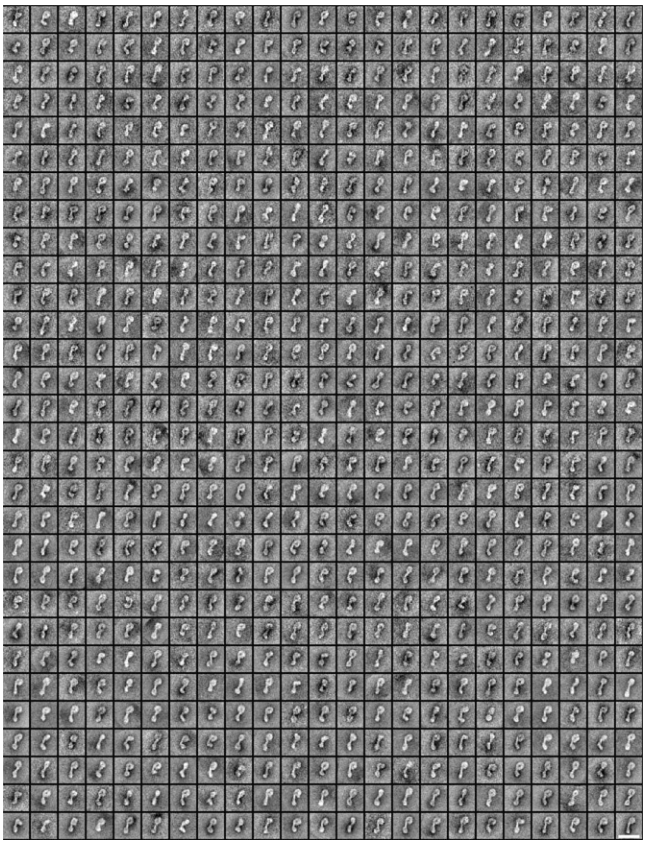

Fig. S2. Classification of HOPS (Vps39-GFP). A total of 24,900 HOPS (Vps39-GFP) particles were selected. The images were aligned and classified into 690 classes using reference-free alignment and *k*-means classification procedures, as described in *SI Experimental Procedures*. (Scale bar, 50 nm.)

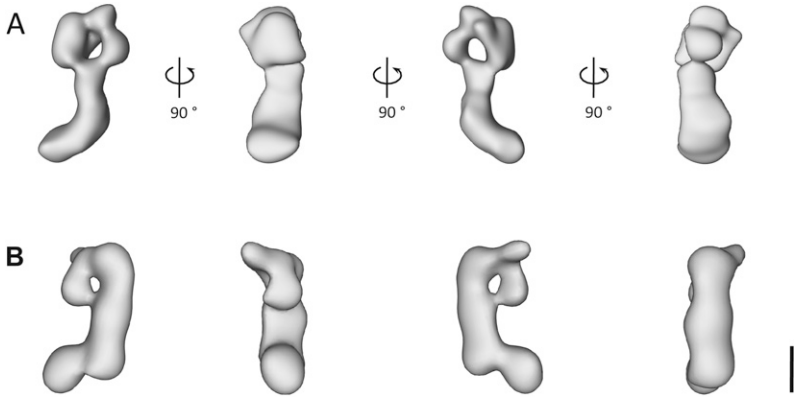

Fig. S3. 3D reconstructions of single HOPS complexes derived from tomograms of negatively and cryo-negatively stained samples. Tomograms of HOPS single particles were collected from (*A*) negatively stained and (*B*) cryo-negatively stained samples, and reconstructions of single HOPS complexes were calculated as described in *SI Experimental Procedures*. (Scale bar, 10 nm.)

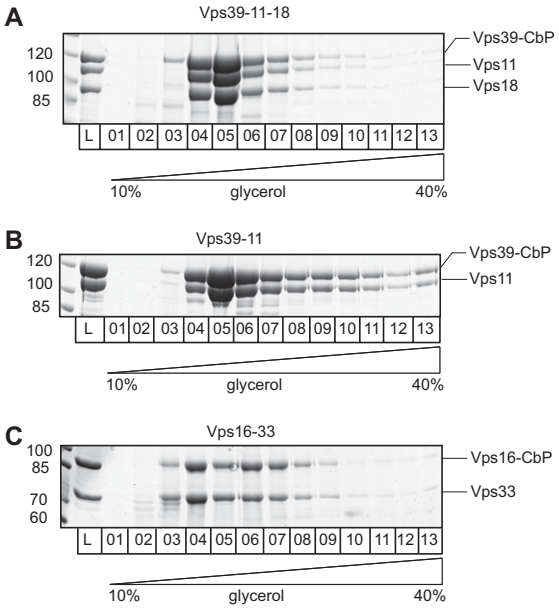

Fig. S4. Enrichment of three HOPS subcomplexes by glycerol gradient centrifugation. TAP-tagged Vps39 (*A* and *B*) and Vps16 (*C*) were purified from the respective co-overexpression strain via IgG beads and eluted by TEV-protease cleavage. Eluates were loaded onto a 10–40% glycerol gradient and centrifuged (*SI Experimental Procedures*). Protein complexes present in the peak fractions were subjected to single-particle analyses. (*A*) Vps39-Vps18-Vps11 complex, (*B*) Vps39-Vps11 complex, (*C*) Vps16-Vps33 complex. CbP remains after TEV cleavage on the tagged protein.

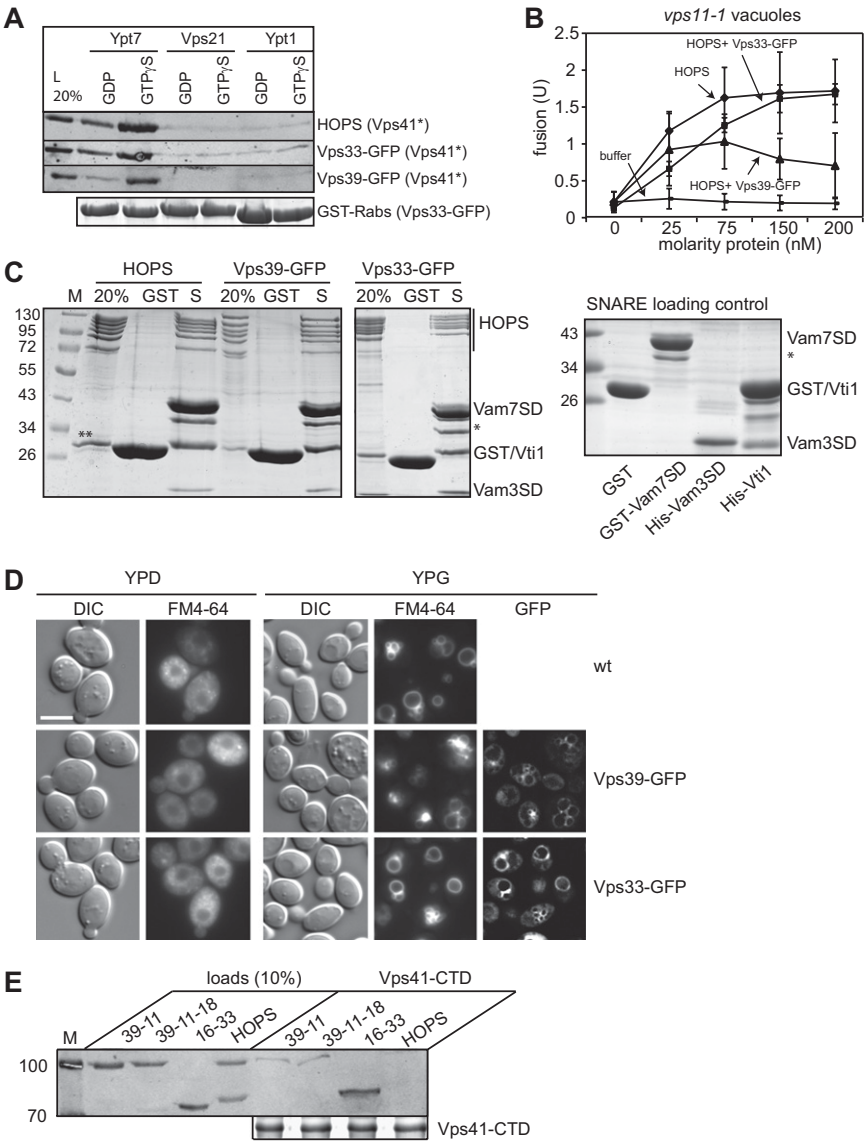

Fig. S5. Functionality assay of HOPS and GFP-tagged HOPS variants. (*A*) HOPS binding to Ypt7-GTP. Control HOPS, as well as HOPS with GFP-tagged Vps33 or Vps39, were purified via the TAP-tag on Vps41 and subjected to GST pull-down with nucleotide-loaded Ypt7 and Vps21 (*SI Experimental Procedures*). Eluates were subjected to SDS/PAGE and Western blotting against CbP. A representative Coomassie-stained gel of GST-Rabs is shown below. (*B*) Fusion activity. Fusion was performed as in Fig. 1*D*, except that different concentrations of HOPS variants were added (*1*). Shown are SDs, $n = 3$. (*C*) Interaction of HOPS with the assembled minimal SNARE complex. SNAREs (Vam3 SNARE domain, Vti1, Nyv1) were incubated with GST-Vam7 SNARE domain or GST, and washed. Purified HOPS complexes were added to the SNAREs, incubated, and proteins were eluted by boiling in SDS sample buffer. Eluates were resolved on SDS/PAGE gels and stained with Coomassie. Purified SNARE proteins and GST are shown to the right (1); * and ** indicate bands of Vam7SD degradation and TEV protease, respectively. (*D*) Vacuole morphology. Overexpression strains without or with GFP-tagged HOPS subunits were grown in YPD or YPG, stained with FM4-64 (*SI Experimental Procedures*), and analyzed by fluorescence microscopy. DIC, differential interference contrast. (Scale bar, 5 μm.) (*E*) Interaction of Vps41 with the Vps16-33 subcomplex. His_6-tagged Vps41 (residues 497–900; Vps41-CTD) was purified and immobilized on Ni-NTA beads and then incubated with the indicated purified subcomplexes or HOPS. Proteins were eluted by boiling in SDS sample buffer, resolved on SDS/PAGE gels, and analyzed by Western blotting using an antibody against CbP. An aliquot of the eluate was analyzed on Coomassie-stained gels to show His_6-Vps41-CTD.

1. Krämer L, Ungermann C (2011) HOPS drives vacuole fusion by binding the vacuolar SNARE complex and the Vam7 PX domain via two distinct sites. *Mol Biol Cell* 22:2601–2611.

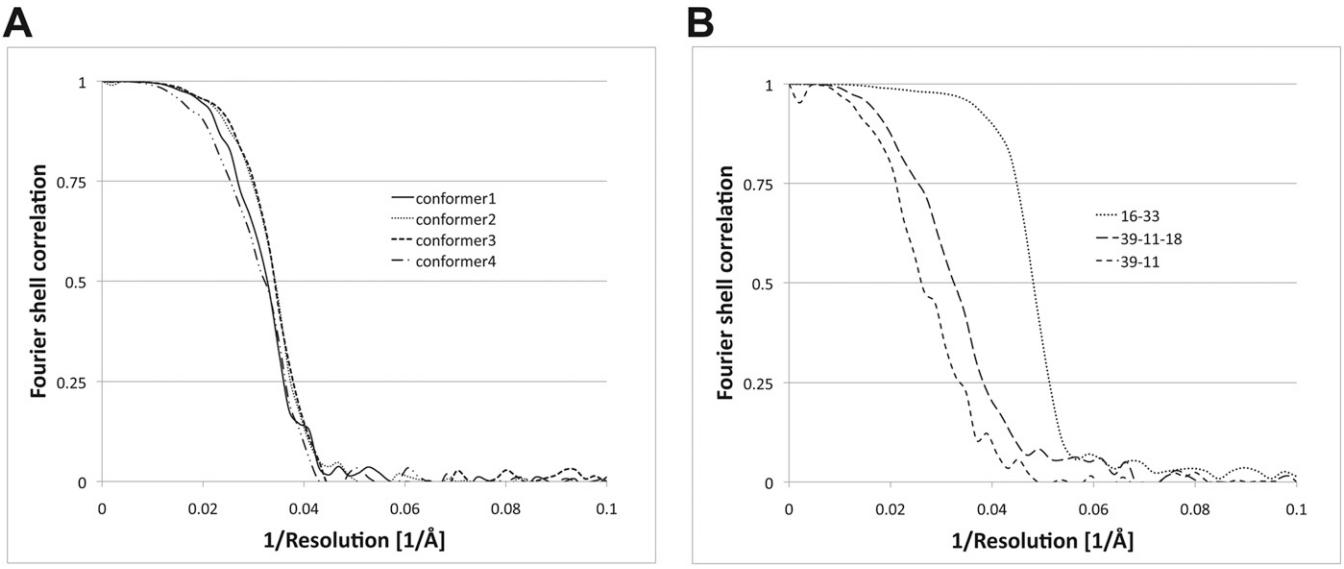

Fig. S6. Fourier shell correlations. Fourier shell correlations of (*A*) the four different reconstructions of the HOPS complex presented in Fig. 1 and of (*B*) the three different subcomplexes Vps16-33, Vps39-11-18, and Vps39-11, shown in Fig. 2.

Table S1. Comparison of volumes

Fig. 1*E*	Fig. 1*F*	Fig. 1*G*	Fig. 1*H*	Average
1,543 Å^3	1,545 Å^3	1,507 Å^3	1,554 Å^3	1,537 ± 21 Å^3

Volumes of the structures in Fig. 1 *E–H* measured at the same density threshold in Chimera are very similar, indicating that the structures have the overall same composition.

Table S2. Yeast strains used in this study

Strain	Genotype	Reference
CSY09	*vps11Δ::HIS3MX6 pep4Δ::KanMX6 VPS11-1ts-URA3*	(1)
CSY10	*vps11Δ::HIS3MX6 pho8Δ::KanMX6 VPS11-1ts-URA3*	(1)
CUY2675	BY4732xBY4727 *VPS41::TRP1-GAL1pr VPS41::TAP-URA3 VPS39::KanMX6-GAL1pr VPS33::HIS3-GAL1pr VPS11::HIS3-GAL1pr VPS16::natNT2-GAL1pr VPS18::KanMX6-GAL1pr-3HA*	(2)
CUY2724	BY4727 *VPS39::natNT2-GAL1pr VPS39::TAP-URA3 VPS11::HIS3-GAL1pr*	(3)
CUY3238	BY4733xBY4732 *VPS33::HIS3-GAL1pr VPS16::KanMX6-GAL1pr VPS16::TAP-URA3*	This study
CUY3396	BY4727 *VPS11::HIS3-GAL1pr VPS39::natNT2-GAL1pr VPS39::TAP-URA3 VPS18::TRP1-GAL1pr*	(2)
CUY4391	BY4732xBY4727 *VPS41::TRP1-GAL1pr VPS41::TAP-URA3 VPS39::KanMX6-GAL1pr VPS39::yeGFP-hphNT1 VPS33::HIS3-GAL1pr VPS11::HIS3-GAL1pr VPS16::natNT2-GAL1pr VPS18::KanMX6-GAL1pr-3HA*	This study
CUY4395	BY4732xBY4727 *VPS41::TRP1-GAL1pr VPS41::TAP-URA3 VPS39::KanMX6-GAL1pr VPS33::HIS3-GAL1pr VPS33::yeGFP-hphNT1 VPS11::HIS3-GAL1pr VPS16::natNT2-GAL1pr VPS18::KanMX6-GAL1pr-3HA*	This study

1. Stroupe C, Collins KM, Fratti RA, Wickner W (2006) Purification of active HOPS complex reveals its affinities for phosphoinositides and the SNARE Vam7p. *EMBO J* 25:1579–1589.
2. Ostrowicz CW, et al. (2010) Defined subunit arrangement and rab interactions are required for functionality of the HOPS tethering complex. *Traffic* 11:1334–1346.
3. Cabrera M, et al. (2009) Vps41 phosphorylation and the Rab Ypt7 control the targeting of the HOPS complex to endosome-vacuole fusion sites. *Mol Biol Cell* 20:1937–1948.

Movie S1. Flexibility of HOPS in 2D.

Movie S1

Movie S2. Flexibility of HOPS in 3D (front view).

Movie S2

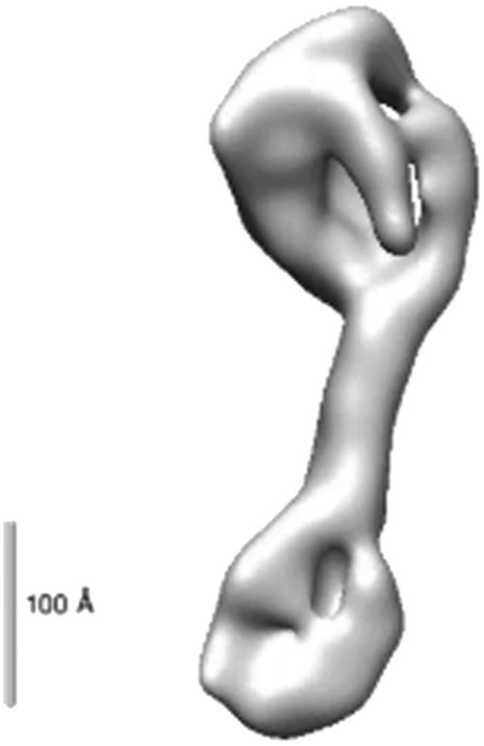

Movie S3. Flexibility of HOPS in 3D (back view).

Movie S3

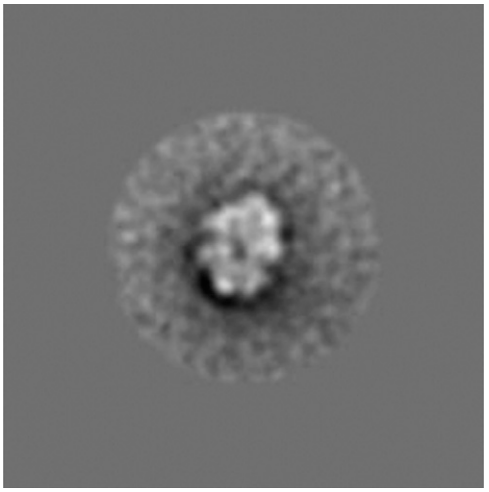

Movie S4. Flexibility of HOPS subcomplex Vps16-Vps33.

Movie S4

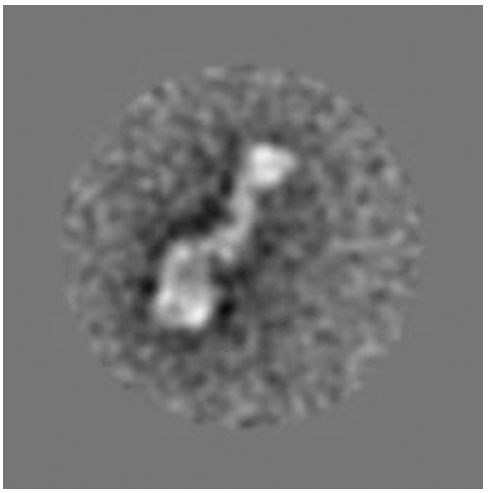

Movie S5. Flexibility of HOPS subcomplex Vps39-Vps11-Vps18.

Movie S5

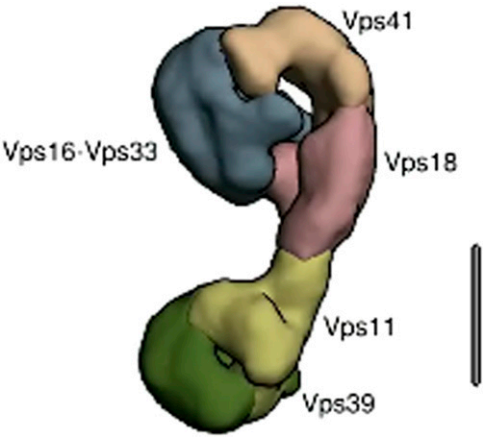

Movie S6. Architecture of the HOPS complex in 3D.

Movie S6